

Effect of actuation sequence on flow rates of peristaltic micropumps with PZT actuators

Ling-Sheng Jang · Kuan Shu · Yung-Chiang Yu ·
Yuan-Jie Li · Chiun-Hsun Chen

Published online: 27 September 2008
© Springer Science + Business Media, LLC 2008

Abstract Many biomedical applications require the administration of drugs at a precise and preferably programmable rate. The flow rate generated by the peristaltic micropumps used in such applications depends on the actuation sequence. Accordingly, the current study performs an analytical and experimental investigation to determine the correlation between the dynamic response of the diaphragms in the micropump and the actuation sequence. A simple analytical model of a peristaltic micropump is established to analyze the shift in the resonant frequency of the diaphragms caused by the viscous damping effect. The analytical results show that this damping effect increases as the oscillation frequency of the diaphragm increases. A peristaltic micropump with three piezoelectric actuators is fabricated on a silicon substrate and is actuated using 2-, 3-, 4- and 6-phase actuation sequences via a driving system comprising a microprocessor and a phase controller. A series of experiments is conducted using de-ionized water as the working fluid to determine the diaphragm displacement and the flow rates induced by each of the different actuation sequences under phase frequencies ranging from 50 Hz to 1 MHz. The results show that the damping effect of actuation sequences influences diaphragm resonant frequency, which in turn affects the profiles of flow rates.

Keywords Peristaltic micropump · Actuation sequence · PZT · Frequency shift

1 Introduction

Advances in the micro-electro-mechanical systems (MEMS) field over the past decade have led to the development of many micropumps, microvalves, micro-mixers and micro-flow sensors designed to manipulate fluids at the micro scale (Cao et al. 2001; Jang and Kan 2007). Of these various devices, micropumps are of vital importance in many biological applications (Laser and Santiago 2004). Various micropumps have been proposed in recent years based on a variety of actuation mechanisms, including piezoelectric (Andersson et al. 2001), shape memory alloys (Shu 2002), electrostatics (Xie et al. 2004; Francais and Dufour 1998), thermal actuation (Tsai and Lin 2002) and rotary magnetics (Ahn and Allen 1995). Of these actuation schemes, the use of piezoelectric actuators is particularly attractive due to their simple structure, high output power density and high actuation force (Nguyen et al. 2002).

In displacement pumps, the energy required to achieve the pumping effect is produced by applying a force to one or more moveable boundaries. Most displacement pumps operate periodically, and incorporate some form of rectifying periodic fluid motion to generate a net flow. Periodic displacement pumps typically utilize either rotary elements, such as gears or vanes, or reciprocating elements such as pistons or diaphragms. Most micropumps are of the latter type and utilize a diaphragm as the moving surface. Peristaltic pumps are a particular class of reciprocating displacement micropump in which the active valves and the primary chambers share a common form (Smits 1990). Peristaltic pumps theoretically require three

L.-S. Jang (✉) · Y.-C. Yu · Y.-J. Li
Department of Electrical Engineering and Center
for Micro/Nano Science and Technology,
National Cheng Kung University,
1 University Road,
Tainan 701, Taiwan
e-mail: lsjang@ee.ncku.edu.tw

K. Shu · C.-H. Chen
Department of Mechanical Engineering,
National Chiao Tung University,
Hsinchu, Taiwan

or more reciprocating membranes, and achieve a pumping effect by applying an appropriate time-controlled actuation sequence to the individual membranes. Such pumps can deliver both air and water, and are characterized by a high bubble tolerance, self-priming and bi-directional transportation characteristics (Husband *et al.* 2004; Lee *et al.* 2004).

In the medical field, a requirement exists for miniaturized pumps to supply small amounts of drugs at a precise and programmable rate for such applications as insulin injection for diabetics, chemotherapy for cancer patients, pain relief for terminally ill patients, and so forth. In peristaltic micropumps, the actuation sequence changes the resonant frequency of the diaphragms, and therefore generates different flow rates. As a result, a single peristaltic micropump can be applied for various applications simply by modifying the actuation sequence. Therefore, investigating the correlation between the actuation sequence and the flow rates is essential in optimizing the performance of a pump and expanding its possible range of applications without the need to redesign the pump or to supply additional electrical energy. Smits presented a peristaltic micropump with three valves actuated peristaltically using a 6-phase actuation sequence (Smits 1990). Husband *et al.* developed a polymerase chain reaction (PCR) microdevice featuring an integrated peristaltic pump and reaction chamber in which the micropump was actuated using a 6-phase sequence (Husband *et al.* 2004). Lee *et al.* fabricated a bidirectional valveless peristaltic micropump for immunoassay applications in which the actuators were driven piezoelectrically via a 3-phase actuation sequence (Lee *et al.* 2004).

However, while the literature contains many proposals for diaphragm pumps of various designs, very little data exists regarding the effect of the actuation sequence on the flow rates of peristaltic micropumps driven by PZT (Lead Zirconate Titanate oxide) actuators. Accordingly, the current study performs an analytical and experimental investigation to determine the correlation between the dynamic response of the diaphragms in the micropump and the actuation sequence. Using a simple mathematical model of the diaphragm within a peristaltic micropump, an analytical formulation is derived to express the viscous damping constant acting on the diaphragm as a function of the actuation sequence. A peristaltic micropump with three PZT actuators is fabricated on a silicon substrate and is actuated using 2-, 3-, 4- and 6-phase actuation sequences produced by a driving system comprising a microprocessor and a phase controller. A series of experiments are performed using de-ionized water to investigate the correlation between the actuation sequence, the resonant frequency of the diaphragm and the flow rates, respectively.

2 Actuation sequences

In analyzing the correlation between the actuation sequence and the resonant frequency of the diaphragm, this study considers the case of a micropump comprising three chambers with integrated PZT/Pyrex diaphragms. The electrical signals required to actuate the diaphragms are generated by three differential amplifiers and a phase controller operating under the control of a microprocessor. As shown in Fig. 1, the present analyses consider four different actuation sequences, namely 6-phase, 4-phase, 3-phase and 2-phase, respectively. The 6-phase sequence is annotated as 100-110-010-011-001-000, where “1” indicates that the corresponding diaphragm is actuated and is in the “up” position, resulting in fluid being drawn into the chamber, while “0” indicates that the diaphragm is in the “down” position, thereby pushing the fluid out of the chamber. As shown in the figure, in the 6-phase sequence, fluid is drawn into the pump in steps 1–3 and is pumped out in steps 4–6. The 4-phase sequence omits steps 010 and 000 in the 6-phase sequence and is annotated as 100-110-011-001. Meanwhile, the 3-phase sequence skips steps 110, 011 and 000 in the 6-phase sequence and is annotated as 100-010-001. Finally, the 2-phase sequence has just two steps, i.e. 000-111. Figure 2 illustrates the driving voltage profiles applied to the three actuators in the micropump under each of the four actuation sequences. Table 1 presents the cycle frequency for each of the actuation sequences. Note that in this table, the phase frequency is defined as $1/T_j$, the cycle duration T represents the sum of all T_j in the phase sequence, and the cycle frequency is given by $1/T$.

In Table 1, the cycle frequency is equivalent to the number of diaphragm oscillations in a given period. Assuming that the phase frequency is assigned a value of 120 Hz, Table 1 shows that the cycle frequencies of the 2-, 3-, 4- and 6-phase actuation sequences are 60, 40, 30 and 20, respectively. In other words, the oscillation frequency of the 2-phase sequence is greater than that of the 3-, 4- or 6-phase sequences. A cycle frequency factor (α) is used to quantify the relationship between the actuation sequence and the oscillation frequency of the diaphragm and is computed by normalizing the oscillation frequencies of the four sequences with respect to that of the two-phase sequence, as shown in Table 2.

3 Driving circuit

Figure 3 presents a block diagram of the driving system used in the current study to actuate the micropump. As shown, the system comprises an ATmega 8535 microprocessor, a high-voltage power supply, three differential amplifiers, an LCD display module, an A/D converter, a

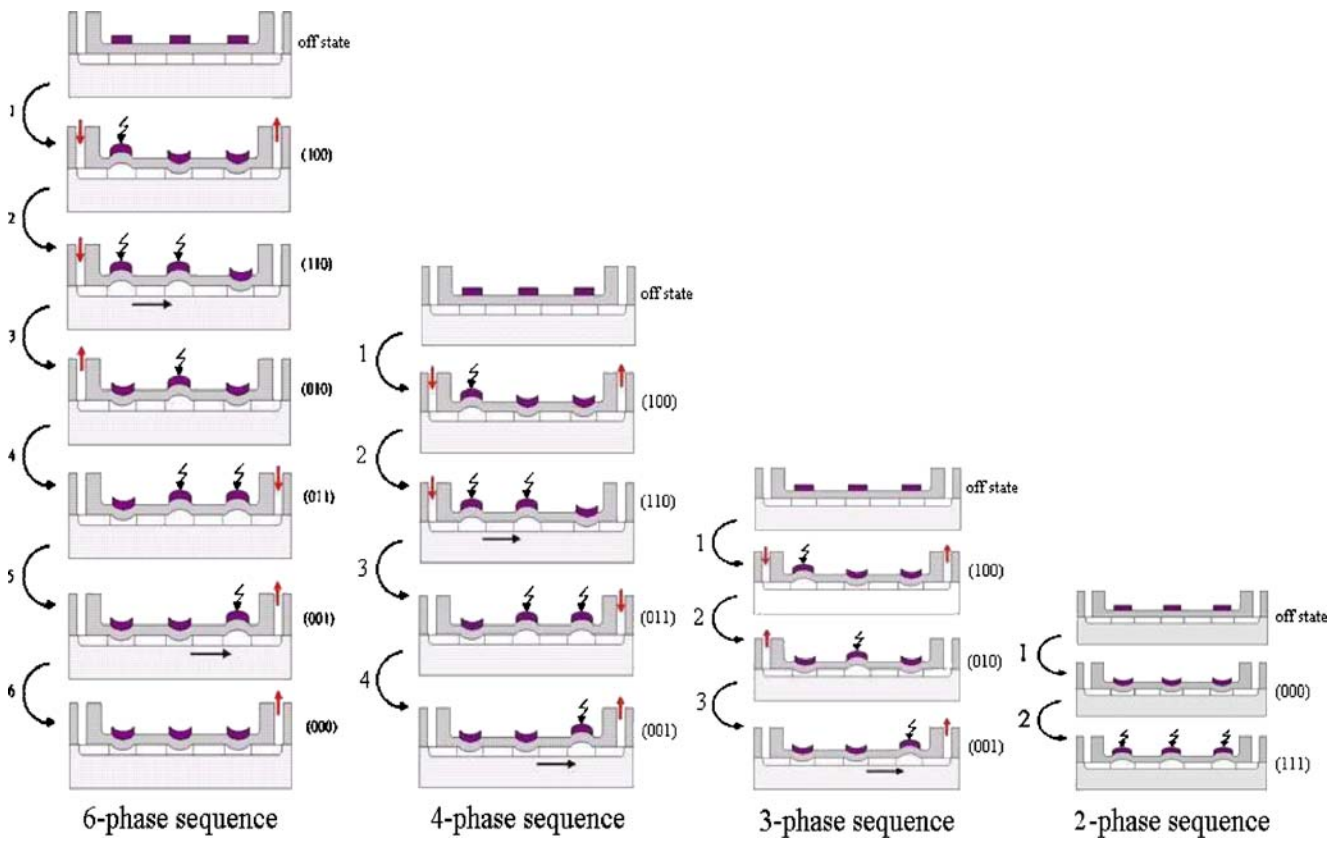


Fig. 1 Four actuation sequences of peristaltic micropump with PZT actuators

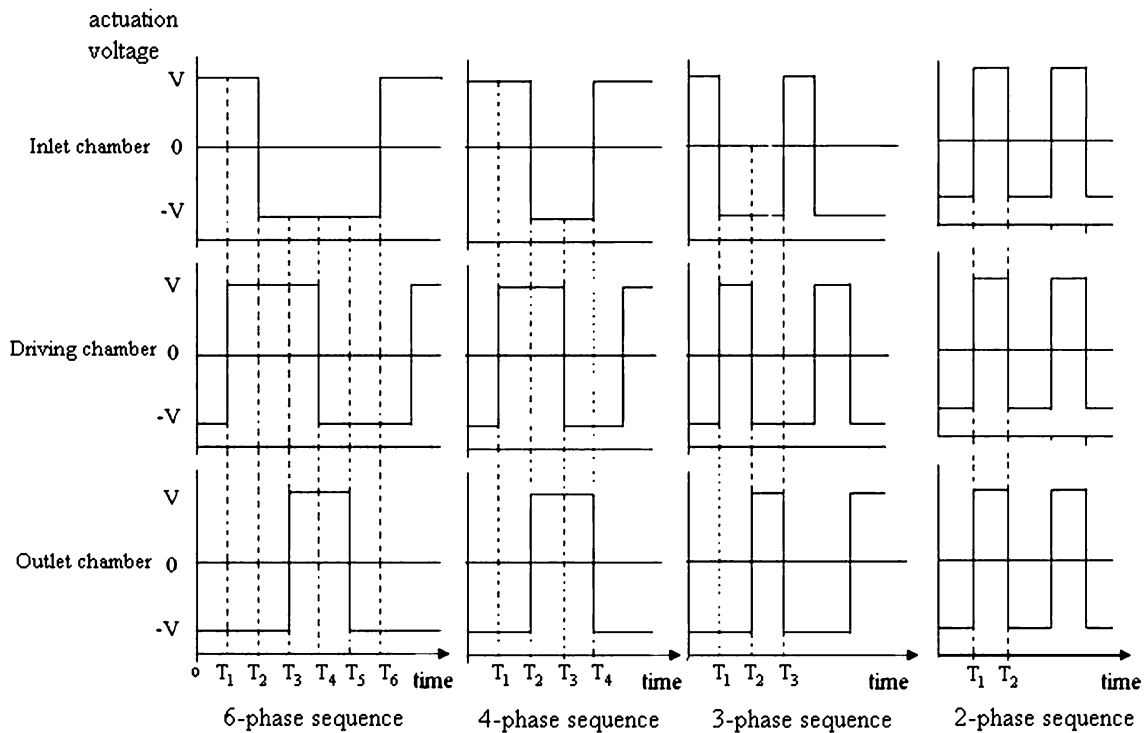


Fig. 2 Duration of phase sequences

Table 1 Cycle frequency of different actuation sequences for given phase frequency

Actuation sequence	Phase duration (s)	Cycle duration (s)	Cycle frequency (1/s)
2-phase	T_j	$2 T_j$	$1/(2 T_j)$
3-phase	T_j	$3 T_j$	$1/(3 T_j)$
4-phase	T_j	$4 T_j$	$1/(4 T_j)$
6-phase	T_j	$6 T_j$	$1/(6 T_j)$

phase controller and a 555 oscillator (Jang and Yu 2008). The driving system is designed to generate step-function signals with voltages of up to $100 V_{pp}$ and frequencies ranging from 10 Hz to 1 kHz. The heart of the driving system is the ATmega microprocessor with a high-performance, low-power AVR[®] 8-bit microcontroller (manufactured by ATMEL). The microprocessor features a self-programmable memory, multiple instructions and a debugging interface. The control code used to actuate the micropump is written in C programming language and is embedded in the microprocessor. During the pumping operation, the LCD module receives character codes from the microprocessor and latches these codes to its display data RAM. Each character code is then transformed into the corresponding character or digit and displayed on the LCD screen. The high-voltage power supply is fed by a 110 Vrms 60 Hz AC line and utilizes a linear technique to generate an output voltage, which is then supplied to the differential amplifiers. The output voltage of the power supply is also processed by a CMOS 8-bit successive approximation A/D converter (ADC0804) in order to transform the analog DC voltage signal into a digital equivalent. The voltage values from the A/D converter are then displayed on the LCD display screen together with the phase frequency values received from the 555 oscillator. The output of the differential amplifiers is twice that of the DC input when the phase controller provides reverse signals to their base terminals (Carr and Brown 2001; Gopalan 1996). The amplifier circuit amplifies the signals applied between its two inputs and rejects any noise signals common to both inputs. The phase controller comprises three clocked D flip-flops controlled by the 555 oscillator, and provides signals to the input terminals of the differential amplifiers in accordance with the instructions received from the microprocessor. The circuits of the three differential amplifiers are designed to process the six signals produced by the phase controller in such a way as to generate a 2-, 3-, 4- or 6-phase actuation sequence.

4 Design and fabrication

Figure 4 presents a schematic illustration of the peristaltic micropump fabricated in this study. As shown, the micro-

pump consists of a silicon substrate, a Pyrex upper plate and three commercially available bulk PZT chips (Bu et al. 2003). The Pyrex plate was etched using a photolithography process with 49% HF to form a rectangular diaphragm with a thickness of 200 μm . Using a diamond bit, two holes were then drilled at either end of the Pyrex plate to create the inlet and outlet channels of the micropump, respectively. The pump channels and chambers were fabricated on a silicon (100) substrate with a thickness of 500 μm using a two-stage etching process. In the first stage, an aluminum layer with a thickness of 3000 \AA was sputtered onto the silicon substrate and the main channel of the micropump was patterned using a photolithography process. A deep reactive ion etching (DRIE) process was then performed using an aluminum etchant to form a channel with a depth of 170 μm . The photolithography and DRIE processes were then repeated to pattern three chambers, each with a depth of 30 μm and a diameter of 12 mm. (Note that this etching process resulted in the depth of the microchannel increasing to 200 μm). The Pyrex membrane was bonded to the patterned silicon substrate using an anodic bonding process performed at a temperature of 475°C with a voltage of 1000 V. Three 12 mm \times 12 mm PZT chips (T107-H4E-602, Piezo Systems, Inc.) with a thickness of 191 μm were then attached to the glass diaphragm using silver epoxy glue (H31, EPO-TEK). Finally, an electric connector and two inlet and outlet tubes were attached to the pump body using epoxy glue. As shown in Fig. 4, the overall dimensions of the assembled pump were 75 mm \times 24 mm \times 1.1 mm.

5 Analysis of actuation sequence effect on resonant frequency of diaphragm

Figure 5(a) presents the simple spring-mass-damper model used in the present study to analyze the dynamic behavior of the PZT/Pyrex diaphragm when actuated by the driving system. The system response can be described as follows:

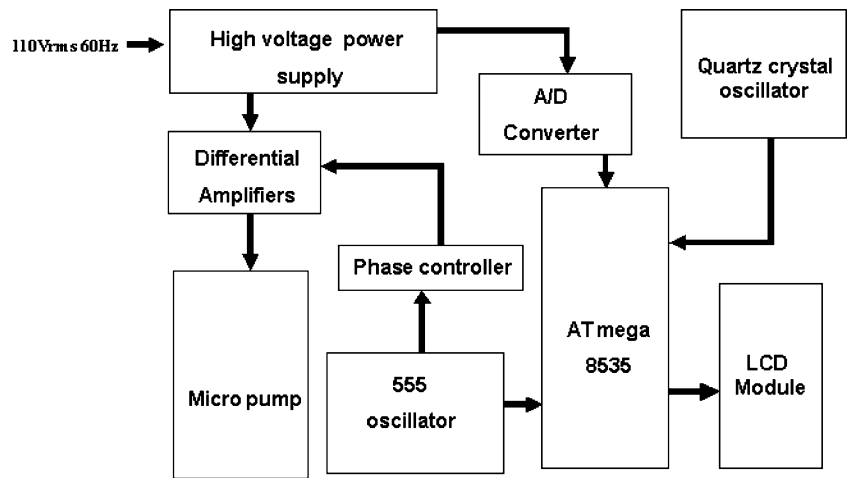
$$M\ddot{y} + ky = \bar{F} \sin(\omega t) - F_{\text{chamber}}, \quad (5.1)$$

where \bar{F} is the force generated by the PZT actuator, ω is the angular frequency, F_{chamber} is the fluid force acting on the

Table 2 Cycle frequency factor (α)

Actuation sequence	Cycle frequency factor
2-phase	$1/(2 T_j)=1$
3-phase	$1/(3 T_j)=0.67$
4-phase	$1/(4 T_j)=0.5$
6-phase	$1/(6 T_j)=0.33$

Fig. 3 Block diagram of driving system



diaphragm, and M and k are the mass and spring constant, respectively. The solution to the homogeneous part decays exponentially with time and is initially significant. The particular solution is a steady-state oscillation having the same frequency as that of the excitation, i.e.

$$y = A_d \sin(\omega t - \phi), \dot{y} = \omega A_d \cos(\omega t), \quad (5.2)$$

where A_d and ϕ denote the frequency-dependent amplitude of the diaphragm and the phase shift, respectively. The analytical model assumes the diaphragm to be actuated by a sinusoidal waveform. In practice, any physical periodic phenomenon can be represented by an infinite sum of harmonically related sinusoids. Therefore, the frequency response of a system to a sinusoidal input provides an

indication of its response to a variety of periodic inputs, including the step-function driving signals applied in the current micropump. The central task is to define the flow resistance acting on the diaphragm.

Figure 5(b) presents a simplified model of the central diaphragm in the current micropump for the case where a viscous liquid is driven through the narrow gap between the pump at a volume flow rate of Q (Fox and McDonald 1990). Note that the flow rate is assumed to have a low value such that the flow is laminar and the pressure gradient associated with the convective acceleration in the narrow gap between the pump body and the diaphragm is negligible compared to that associated with the viscous forces. Furthermore, the velocity profile at any cross-section in the gap is assumed to be equivalent to that of a

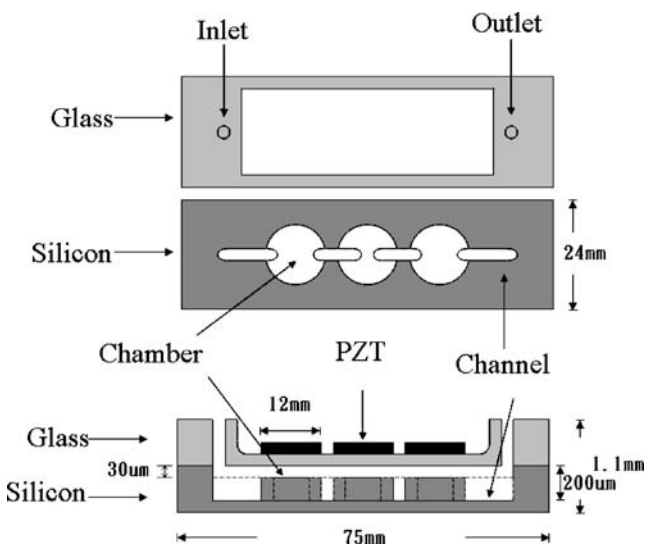


Fig. 4 Schematic illustration of peristaltic micropump with piezoelectric actuators

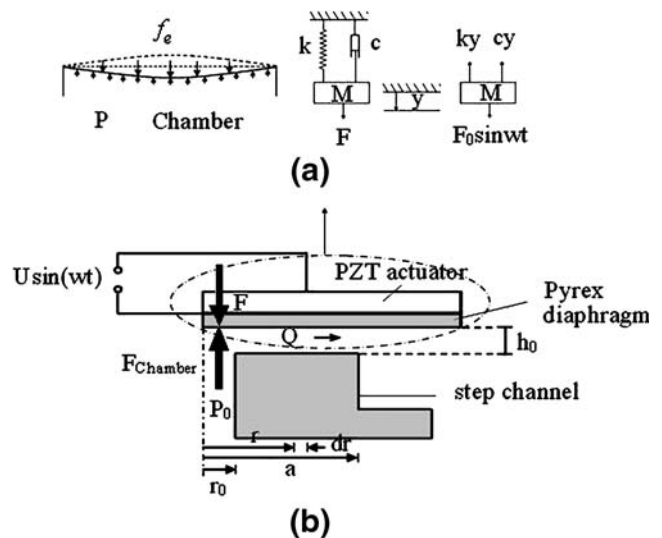
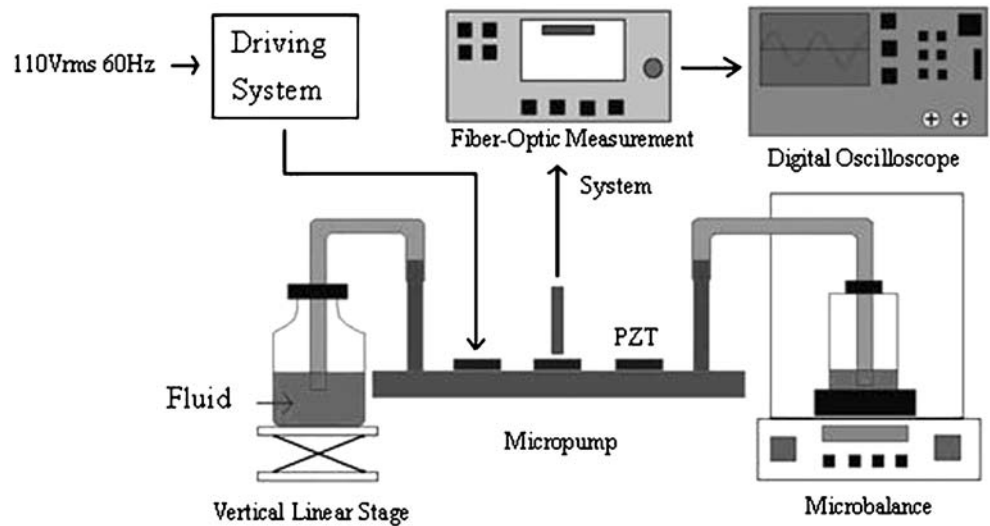


Fig. 5 (a) Simplified model of viscously damped diaphragm micropump under harmonic excitation. (b) Simplified model of diaphragm micropump

Fig. 6 Schematic illustration showing experimental setup



fully developed flow between two stationary parallel plates, i.e. the flow has an axi-symmetric velocity profile. Hence, the control volume is in the form of an annulus with a width dr and a circumference $2\pi r$.

The pressure gradient within the gap, dp/dr , can be expressed as a function of the annulus radius as follows:

$$\frac{Q}{2\pi r} = -\frac{1}{12} \left(\frac{dp}{dr} \right) h_0^3 \Rightarrow \frac{dp}{dr} = -\frac{6\mu Q}{\pi h_0^3 r} \quad (5.3)$$

Meanwhile, the flow rate Q can be approximated as:

$$Q = \pi(a^2 - r^2) \dot{y} \quad (5.4)$$

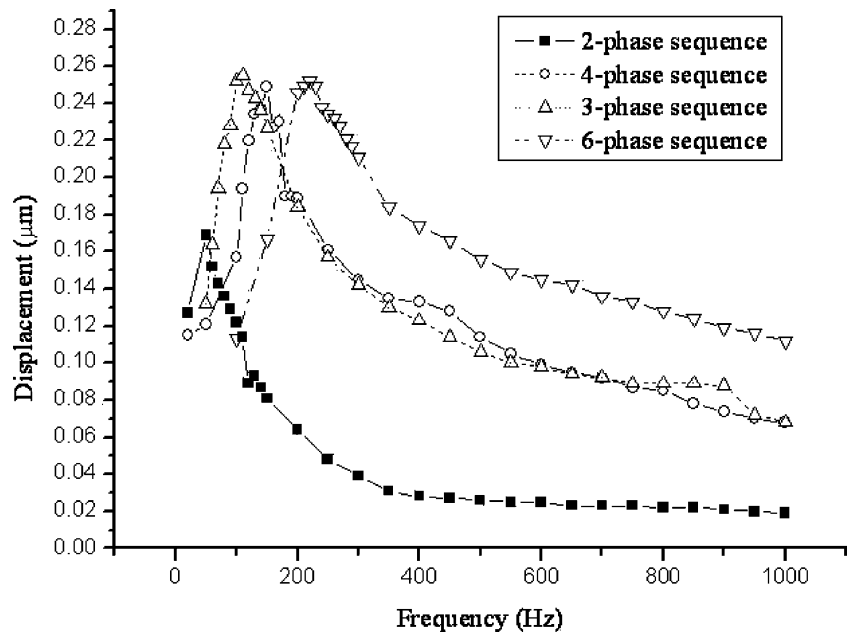
Substituting Eq. 5.4 into Eq. 5.3 and integrating the result, it can be shown that the pressure distribution in the narrow gap in Fig. 5(b) has the form:

$$P = P_0 + \frac{6\mu \dot{y}}{h_0^3} \left(a^2 \ln \frac{r}{a} - \frac{1}{2} r^2 + \frac{1}{2} a^2 \right), \quad (r_0 < r < a) \quad (5.5)$$

The flow resistance acting on the diaphragm is given by $F_{\text{chamber}} = \int_0^a p(r) 2\pi r dr$, and thus the force acting on the diaphragm can be derived as:

$$F_{\text{chamber}} = \pi a^2 p_0 + \frac{12\pi\mu \dot{y}}{h_0^3} \times \left\{ a^4 \left[\frac{1}{4} + \frac{1}{2} \left(\frac{r_0}{a} \right)^2 \right] \left[\ln \left(\frac{r_0}{a} \right) - \frac{1}{2} \right] - \frac{1}{8} (a^2 - r_0^2)^2 \right\} \quad (5.6)$$

Fig. 7 Variation of diaphragm displacement with phase frequency for 2-, 3-, 4- and 6-phase actuation sequences. Note that the driving voltage is 20 V_{pp} in every case and the working fluid is air



The viscous damping constant is proportional to the diaphragm velocity and can be obtained from Eq. 5.6 and the cycle frequency factor α , i.e.

$$c = \frac{\alpha \cdot 12\pi\mu a^4}{h_0^3} \times \left\{ \left[\frac{1}{4} + \frac{1}{2} \left(\frac{r_0}{a} \right)^2 \right] \left[\ln \left(\frac{r_0}{a} - \frac{1}{2} \right) \right] - \frac{1}{8a^4} (a^2 - r_0^2)^2 \right\}. \tag{5.7}$$

where α has a value of 1, 0.67, 0.5 and 0.33 for the 2-, 3-, 4- and 6-phase sequences, respectively (see Table 2). From Eq. 5.7, it can be seen that the damping effect are dependent upon four main parameters, namely the fluid viscosity (μ), the chamber depth (h_0), the diaphragm length (a) and the geometric constant ($\ln(\frac{r_0}{a})$). Substituting Eq. 5.7 into Eq. 5.6 yields the following equation:

$$F_{\text{chamber}} = \pi a^2 p_0 + c \dot{y}. \tag{5.8}$$

Therefore, by rearranging Eq. 5.1 using Eq. 5.8, expression for the dynamic behavior of the diaphragm can be obtained as:

$$M \ddot{y} + c \dot{y} + ky = \bar{F} \sin(\omega t) - \pi a^2 p_0. \tag{5.9}$$

The magnitude of the transfer function for a forced-excitation system such as that shown in Fig. 5 is given by:

$$A_d = |g(\omega)| = \frac{\bar{F} - \pi a^2 p_0}{M} \frac{1}{\sqrt{(\omega_n^2 - \omega^2)^2 + (2\zeta\omega\omega_n)^2}}, \tag{5.10}$$

where $\omega_n^2 = \frac{k}{M}$ and $\zeta = \frac{c}{2\sqrt{Mk}}$.

The frequency at which the amplitude–response curve attains its maximum position (referred to as the damped natural frequency, ω_d) can be obtained by differentiating Eq. 5.10 with respect to ω and setting the result equal to zero, i.e.

$$\omega_d = \omega_n \sqrt{1 - 2\zeta^2} = \omega_n \sqrt{1 - \frac{c^2}{Mk}}, \tag{5.11}$$

where $\omega_n = \sqrt{\frac{k}{M}}$ is the natural frequency of the diaphragm in a vacuum and $\zeta = \frac{c}{2\sqrt{Mk}}$ is the damping factor (Timoshenko and Weaver 1974). According to Eqs. 5.11 and 5.7, the resonance peak occurs at a frequency lower than the undamped natural frequency ω_n . From Eq. 5.11, it can be seen that the reduction in the resonant frequency of the diaphragm increases as the damping effect related to the cycle frequency factor increases.

6 Results and discussion

To evaluate the effect of the actuation sequence on the pump performance, the pump was excited via 2-, 3-, 4- and 6-phase actuation sequences using step-function signals with various driving voltages and frequencies. Figure 6 presents a schematic illustration of the experimental setup. As shown, the end of the outlet tube was placed in a reservoir positioned on a microbalance such that the pumping rate could be computed by measuring the change in the weight of the DI water in the reservoir over a specified period (1 min in the current experiments). The maximum displacement of the central diaphragm was measured using a fiber-optical measurement system (MTI 2000, MTI Instruments) with an accuracy of within 1.0%

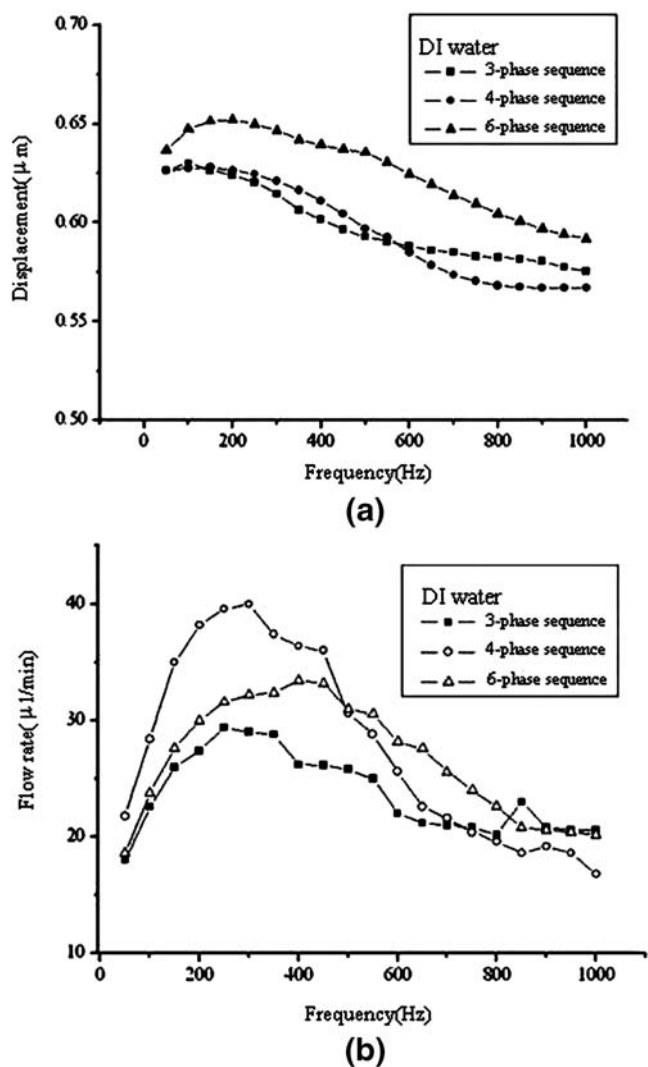


Fig. 8 (a) Variation of diaphragm displacement with phase frequency for 3-, 4- and 6-phase actuation sequences. (b) Variation of flow rate with phase frequency for 3-, 4-, and 6-phase actuation sequences. Note that the driving voltage is 100 V_{pp} in every case and the working fluid is DI water

for peak-to-peak readings from 1 Hz to 150 kHz. The displacement of the diaphragm was visualized using a digital oscilloscope. The flow rates were obtained from the various actuation sequences at a zero backpressure. The experiments were all performed at a constant temperature of 25°C.

Figure 7 illustrates the variation of the diaphragm displacement as a function of the phase frequency for each of the four actuation sequences. Note that the driving voltage is 20 V_{pp} in each case and the working fluid is air. The results confirm that the resonant frequency of the diaphragm depends on the actuation sequence. From inspection, the resonant frequencies of the diaphragm are found to be 50, 110, 150 and 220 Hz when the PZT chips are excited via the 2-, 3-, 4- and 6-phase actuation sequences, respectively. In other words, the results show that the resonant frequency increases as the cycle frequency factor reduces. This result is to be expected since Eq. 5.7 shows that the damping constant reduces as the cycle frequency factor reduces.

Figure 8(a) illustrates the variation of the diaphragm displacement as a function of the actuation frequency when using DI water as the working fluid. (Note that the 2-phase actuation sequence does not yield a net flow, and thus the corresponding displacement data are deliberately omitted here). The resonant frequencies of the diaphragm are found to be 100, 150 and 200 Hz, respectively, when the micropump is actuated using the 3-, 4- and 6-phase sequences. Figure 8(b) shows the variation of the flow rates with the excitation frequency when the micropump is actuated using a driving voltage of 100 V_{pp}. From inspection, the maximum flow rates are found to be 29.2 µl/min at 250 Hz (3-phase sequence), 40.1 µl/min at 300 Hz (4-phase sequence) and 33.5 µl/min at 400 Hz (6-phase sequence), respectively. According to the analysis, the damping effect of actuation sequences influenced diaphragm resonant frequency, which in turn affected the profiles of flow rates.

7 Conclusion

This study has performed an analytical and experimental investigation to examine the correlation between the actuation sequence used to excite a peristaltic micropump, the resonant frequency of the diaphragm and the flow rates. Using a simple analytical model of the diaphragm within the micropump, it has been shown that the additional damping depends on the actuation sequence applied. The results show that the reduction in the resonant frequency of

the diaphragm increases as the damping effect related to the cycle frequency factor increases. The effect of the actuation sequence on the resonant frequency of the diaphragm and the profiles of the flow rates has been investigated experimentally using de-ionized water as the working fluid. The experimental results have revealed that the resonant frequency of the diaphragm and the flow rates are both affected by the actuation sequence.

Acknowledgements This study was supported by the National Science Council of Taiwan under Grant No. NSC 93-2215-E-006-021. The authors would like to thank the Center for Micro/Nano Science and Technology, National Cheng Kung University, and National Nano Device Laboratories, Tainan, Taiwan, for the access granted to major items of equipment and their provision of technical support throughout the course of the study. Additionally, this study utilized shared facilities supported by the Top 100 Universities Advancement Program managed by the Ministry of Education, Taiwan.

References

- C.H. Ahn, M.G. Allen, Fluid micropumps based on rotary magnetic actuators. *Proceedings of the IEEE Micro Electro Mechanical Systems (MEMS)*. 408–412 (1995)
- H. Andersson, W. van der Wijngaart, P. Nilsson, P. Enoksson, G. Stemme, A valve-less diffuser micropump for microfluidic analytical systems *Sens. Actuators B* **72**, 259–265 (2001)
- M. Bu, T. Melvin, G. Ensell, J.S. Wilkinson, A.G.R. Evans, Design and theoretical evaluation of a novel microfluidic device to be used for PCR *J. Micromechanics Microengineering* **13**(4), S125–S130 (2003), July
- L. Cao, S. Mantell, D. Polla, Design and simulation of an implantable medical drug delivery system using microelectromechanical systems technology *Sens. Actuators A* **94**, 117–125 (2001)
- J.J. Carr, J.M. Brown, *Introduction to Biomedical Equipment Technology*, 4th edn. (Prentice Hall, Upper Saddle River, New Jersey, 2001)
- O. Francais, I. Dufour, Dynamic simulation of an electrostatic micropump with pull-in and hysteresis phenomena *Sens. Actuators A* **70**, 56–60 (1998)
- K.G. Gopalan, *Introduction to Digital Microelectronic Circuits* (IRWIN, Chicago, Michigan, 1996)
- B. Husband, M. Bu, A.G.R. Evans, T. Melvin, Investigation for the operation of an integrated peristaltic micropump *J. Micromech. Microeng* **14**, S64–S69 (2004)
- L.-S. Jang, W.-H. Kan, Peristaltic piezoelectric micropump system for biomedical applications *Biomedical Microdevices* **9**(4), 619–626 (2007)
- L.S. Jang, Y.C. Yu, Peristaltic micropump system with piezoelectric actuators *Microsyst. Technol* **14**(2), 241–248 (2008), February
- D.J. Laser, J.G. Santiago, A review of micropumps *J. Micromechanics Microengineering* **14**(6), R35–R64 (2004), June
- D.S. Lee, H.C. Yoon, J.S. Ko, Fabrication and characterization of a bidirectional valveless peristaltic micropump and its application to a flow-type immunoanalysis *Sens. Actuators B* **103**, 409–415 (2004)

- Fox, McDonald, *Introduction to Fluid Mechanics* (Wiley, New York, 1990)
- N.T. Nguyen, X. Huang, T.K. Chuan, MEMS-Micropumps: A Review *Transaction of the ASME* **124**, 384–391 (2002)
- Y.C. Shu, Shape-memory micropumps *Mater. Trans* **43**(5), 1037–1044 (2002)
- J.G. Smits, Piezoelectric micropump with three valves working peristaltically *Sens. Actuators A* **21–23**, 203–206 (1990)
- S.P. Timoshenko, W. Weaver, *Vibration Problems in Engineering*, 4th edn. (Wiley, New York, 1974)
- J.H. Tsai, L. Lin, Active microfluidic mixer and gas bubble filter driven thermal bubble micropump *Sens. Actuator A* **97–98**, 665–671 (2002)
- J. Xie, J. Shih, Q. Lin, B. Yang, Y.C. Tai, Surface micromachined electrostatically actuated micro peristaltic pump *Lab. Chip* **4**, 495–501 (2004)